Journal of Controlled Release 157 (2012) 103–111

Contents lists available at SciVerse ScienceDirect

Journal of Controlled Release

journal homepage: www.elsevier.com/locate/jconrel

GENE DELIVERY

# Controlled permeation of cell membrane by single bubble acoustic cavitation

Y. Zhou [a], K. Yang [b], J. Cui [c], J.Y. Ye [d,1], C.X. Deng [a,*]

[a] Department of Biomedical Engineering, University of Michigan, Ann Arbor, Michigan 48109-2099, USA
[b] College of Quality and Technical Supervision, Hebei University, Baoding, Hebei, PR China
[c] Department of Biomedical Engineering, Washington University at St. Louis, St. Louis, Missouri, USA
[d] Center for Ultrafast Optical Science and Michigan Nanotechnology Institute for Medicine and Biological Sciences, University of Michigan, Ann Arbor, Michigan, USA

ARTICLE INFO

*Article history:*
Received 2 July 2011
Accepted 10 September 2011
Available online 16 September 2011

*Keywords:*
Sonoporation
Ultrasound
Intracellular delivery
Membrane permeability
Microbubbles
Cavitation

ABSTRACT

Sonoporation is the membrane disruption generated by ultrasound and has been exploited as a non-viral strategy for drug and gene delivery. Acoustic cavitation of microbubbles has been recognized to play an important role in sonoporation. However, due to the lack of adequate techniques for precise control of cavitation activities and real-time assessment of the resulting sub-micron process of sonoporation, limited knowledge has been available regarding the detail processes and correlation of cavitation with membrane disruption at the single cell level. In the current study, we developed a combined approach including optical, acoustical, and electrophysiological techniques to enable synchronized manipulation, imaging, and measurement of cavitation of single bubbles and the resulting cell membrane disruption in real-time. Using a self-focused femtosecond laser and high frequency ultrasound (7.44 MHz) pulses, a single microbubble was generated and positioned at a desired distance from the membrane of a Xenopus oocyte. Cavitation of the bubble was achieved by applying a low frequency (1.5 MHz) ultrasound pulse (duration 13.3 or 40 μs) to induce bubble collapse. Disruption of the cell membrane was assessed by the increase in the transmembrane current (TMC) of the cell under voltage clamp. Simultaneous high-speed bright field imaging of cavitation and measurements of the TMC were obtained to correlate the ultrasound-generated bubble activities with the cell membrane poration. The change in membrane permeability was directly associated with the formation of a sub-micrometer pore from a local membrane rupture generated by bubble collapse or bubble compression depending on ultrasound amplitude and duration. The impact of the bubble collapse on membrane permeation decreased rapidly with increasing distance (D) between the bubble (diameter $d$) and the cell membrane. The effective range of cavitation impact on membrane poration was determined to be $D/d = 0.75$. The maximum mean radius of the pores was estimated from the measured TMC to be $0.106 \pm 0.032$ μm ($n = 70$) for acoustic pressure of 1.5 MPa (duration 13.3 μs), and increased to $0.171 \pm 0.030$ μm ($n = 125$) for acoustic pressure of 1.7 MPa and to $0.182 \pm 0.052$ μm ($n = 112$) for a pulse duration of 40 μs (1.5 MPa). These results from controlled cell membrane permeation by cavitation of single bubbles revealed insights and key factors affecting sonoporation at the single cell level.



## 1. Introduction

Transport of therapeutics, including water-soluble molecules, siRNA and DNAs, into the cells, has emerged as an important area of pursuit in medical, pharmaceutical, and bioengineering research and development. Various approaches have been exploited [1–3], yet efficient intracellular delivery of therapeutics still remains a major challenge.

Acoustic cavitation, with the rapid radial expansion and contraction, and/or collapse of the bubbles driven by the cyclic change of the pressure of an ultrasound field [4], has a unique ability to concentrate energy and forces, and has found utilities in many applications [5,6]. In a biomedical context, acoustic cavitation can generate localized yet significant fluid flow, shear stress, and other mechanical impacts on nearby cells and biological structures [7–10]. Particularly, the localized mechanical impact associated with acoustic cavitation of microbubbles has been recognized as an important factor in ultrasound mediated disruption of cell membrane, or sonoporation [9,11–13]. Such transient disruption of the cell membrane effectively increases the cell membrane permeability and permits easier transport of extracellular compounds that are otherwise impermeable into the cytoplasm of viable cells [11,14–16]. As a physical method that has the ability to localize the delivery within a targeted tissue

* Corresponding author at: Department of Biomedical Engineering, University of Michigan, 2200 Bonisteel Blvd, Ann Arbor, MI 48109-2099, USA. Tel.: +1 734 936 2855; fax: +1 734 936 1905.
*E-mail address:* cxdeng@umich.edu (C.X. Deng).
[1] Current address: Department of Biomedical Engineering, University of Texas at San Antonio, San Antonio, Texas, USA.

0168-3659/$ – see front matter © 2011 Elsevier B.V. All rights reserved.
doi:10.1016/j.jconrel.2011.09.068

volume with minimal inflammatory and immunological responses, sonoporation provides a new and advantageous means for non-viral intracellular drug and gene delivery [17,18]. It can also be used as a versatile strategy for intracellular delivery of a wide range of agents and drug carriers including viral vectors and multi-functional nanoparticles [17,19,20].

However, the technique has been limited by its variable delivery outcome and relatively low delivery efficiency [16,18,21-24]. Although acoustic cavitation has been recognized to facilitate sonoporation, the detailed characteristics of ultrasound-driven microbubble activities and processes involved in sonoporation have not been fully revealed and directly correlated with membrane permeability. Such lack of mechanistic and deterministic knowledge hinders rational determination of sonoporation parameters and other factors to ensure efficacious and consistent outcome.

Precise control of cavitation and assessment of the ensuing sonoporation in a spatiotemporally correlated fashion have been one of the major difficulties in the mechanistic study of sonoporation. The inherently complex, microscopic, dynamic or transient nature of ultrasound interaction with microbubbles makes the task challenging and real-time assessment of the increase of cell membrane permeability in sonoporation is generally unavailable. Thus sonoporation studies have generally relied on post-ultrasound assays, yielding indirect and often largely phenomenological association of ultrasound parameters with delivery outcome.

In this study, an integrated and interdisciplinary approach that combines optical, ultrasonic, and electrophysiology techniques was developed to control ultrasound-driven cavitation of microbubble and activities and measure the resulting change of cell membrane permeability in real-time at the single cell level. Using this method, quantitative correlation of ultrasound-driven microbubble activities and sonoporation was obtained to reveal the key factors involved in sonoporation.

## 2. Materials and methods

### 2.1. Cell model

*Xenopus oocytes* (collegenase-treated and defolliculated from fresh surgically extracted *Xenopus laevis* overies (Nasco, Fort Atkinson, WI)) were used for this study because of their utility as a common cell membrane model system [25].

### 2.2. Experimental setup, generation and control of single microbubble and its cavitation

Fig. 1 shows the experimental setup which includes two separate chambers, one of which was used to house an individual *Xenopus* oocyte (diameter ~0.8 mm) immersed in ND 96 solution (in mM 96 NaCl, 2 KCl, 1.8 $CaCl_2$, 1 $MgCl_2$, 5 HEPES, pH 7.60) to maintain proper physiological environment for the cell. A single oocyte was placed on a small platform in the cell chamber.

A recently developed novel technique [26,27] for generating and trapping of single bubbles using a self-focused (SF) femtosecond (fs) laser beam was employed in this study and combined with an ultrasound technique to achieve spatiotemporal control of cavitation of single microbubbles. The laser beam, generated by a 250 KHz regeneratively amplified Ti:sapphire laser (Coherent, RegA) with a pulse duration of 100 fs and a wavelength of 793 nm, was directed upward and loosely focused (f-number 15) into the cell chamber filled with ND96 solution. The SF fs laser beam generated bubbles via the laser induced optical breakdown (LIOB) and trapped a single bubble (radius 5–12 μm) stably near the focus of the laser [26,27], which was about 500 μm from the oocyte horizontally.

A dual-frequency transducer assembly, consisting of two collinearly and con-focally aligned circular ultrasound transducers (center frequency of 7.44 MHz for the outer transducer and 1.5 MHz for the inner transducer) (Piezo Technologies, Indianapolis, IN), was housed in the chamber adjacent to the cell chamber. Here the transducer chamber was filled with de-ionized water and separated by an acoustically transparent window (Tegaderm transparent dressing, 3M Health Care, St. Paul, MN) from the cell chamber. The transducer assembly was used to generate ultrasound exposures at two different center frequency, duration, and amplitude to spatially control the location and cavitation of a single bubble.

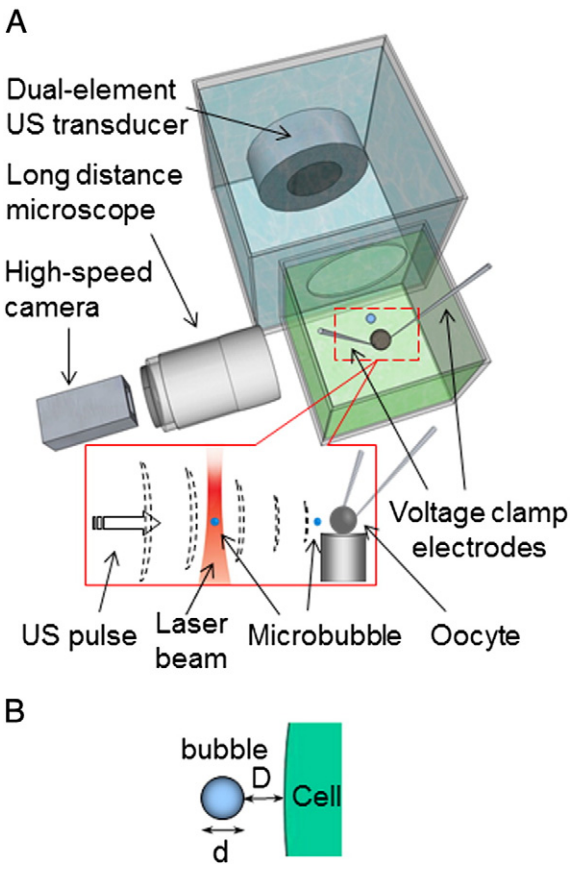


**Fig. 1.** Experimental setup. (A) A single oocyte was placed in ND96 solution. The femtosecond laser beam generated and trapped a single microbubble 500 μm horizontally from the oocyte. An ultrasound transducer assembly in an adjacent tank controlled and generated cavitation. Voltage-clamp measured the TMC of the cell in real time. A high speed camera was used to image the ultrasound-driven dynamic bubble activities. Inset: A microbubble generated by LIOB was trapped and then moved toward the oocyte by the 7 MHz ultrasound pulses. (B) Schematic illustration of the separation distance D between the cell membrane and a bubble (diameter of d).

Operating in pulse-echo mode, the central transducer (diameter of 14 mm; F# 3.9), which was a broad-band transducer (center frequency 7.44 MHz, 50% bandwidth, focal distance 48 mm, 3-dB beam width 0.45 mm), was used to manipulate the bubble position and also monitor its location and status. The transducer generated short ultrasound pulses horizontally aiming at the trapped bubble without destroying it to push the bubble toward the cell membrane by the acoustic radiation of the pulses. It also received echo signals from the bubble from which the movement and location of the bubble can be determined via the M-mode ultrasound image of the bubble.

The donut-shaped, outer transducer (inner and outer diameters of 14 and 30 mm; F# 1.6) was used to generate a focused ultrasound beam at center frequency of 1.5 MHz (focal distance 48 mm, full 3-dB lateral beam width 0.9 mm) to induce oscillation and collapsing of a gas bubble. The bubble activities during the application of the 1.5 MHz ultrasound pulse were imaged by high speed video-microscopy with a long distance microscope (QM 100, Questar, New

Hope, PA) and a high speed camera (Photron Fastcam SA1, Motion Engineering, Indianapolis, IN) with a frame rate of 20–200 KHz.

### 2.3. Measurement of cell membrane permeability

The increase of the membrane permeability induced by ultrasound driven cavitation was assessed by measuring the transmembrane-current (TMC) of the cell with its membrane potential clamped at −50 mV using two microelectrodes, which were glass micropipettes with ~1 μm diameter tip prepared by a micropipette puller (P-87, Sutter Instrument, Novato, CA). The electrodes were inserted into the cytosol of the cell and connected to a voltage clamp amplifier (Dagan CA-1B, Dagan Corp., Minneapolis, MN). In the absence of activation of endogenous ion channels, the TMC was close to zero before the application of the 1.5 MHz ultrasound pulse and cavitation. The voltage clamp was synchronized with ultrasound exposures to allow measurement of the TMC before, during, and after the ultrasound application continuously with a sampling rate >1 KHz.

The short term and medium term viability of the cells after experiments were assessed by the recovered and stable TMC values within 5 min of sonoporation as well as visual observation after the cells were incubated for 24–48 h. Dye exclusion assay using propidium iodide (PI) (668 Da) (Sigma Aldrich, St. Louis, MO) in selected cells (10/200) were also performed. For this assay, PI in a concentration of 100 μM was added to the medium containing the cells after 24–48 h. After 10 min incubation, the cells were washed three times and then frozen. Thin slices (thickness 10 μm) were made through the whole cell and fluorescence microscopic examination of the slices was performed to determine PI uptake to assess the membrane integrity of the cell. These tests were used to confirm cell viability.

### 2.4. Inhibition of pore resealing in sonoporation and scanning electron microscopy (SEM)

As resealing of cell membrane disruption requires extracellular calcium [28–31], the resealing of the pore generated by cavitation can be inhibited by using a calcium free ND 96 solution in the sonoporation experiment while keeping all the other conditions the same. Scanning electron microscopy (SEM) using Quanta™ 3D 200 (FEI company, Hillsboro, Oregon) with low vacuum mode was conducted to examine the cells after the experiment in calcium-free ND 96 solution to confirm pore formation on the cell membrane generated by cavitation of a single bubble. To prepare samples for the SEM, after sonoporation, oocytes were manually devitellinized after being kept in stripping solution (in mM: 200 NMG-Aspartate, 2 KCl, 10 EGTA, 1 $MgCl_2$, 10 HEPES, pH = 7.40) for 2–5 min, and immediately placed again in calcium free ND96 solution with 2.5% Glutaraldehyde at 2–6 °C.

### 2.5. Estimation of the radius of the pores from the TMC

The radius of the pore at any given time point after its formation was estimated from the measured time-dependent TMC using an electro-diffusion model that relates the ion diffusion through pores on the cell membrane under a quasi-steady state assumption [32]. The maximum pore radius that was generated by a bubble at a given separation distance, was calculated from the corresponding maximum amplitude of the TMC.

## 3. Results

### 3.1. Bubble generation and trapping of a single bubble

Microbubbles (radius 3–15 μm) were first generated in the cell chamber filled with ND 96 solution using the upward-directed, self-focusing fs laser beam *via* laser induced optical breakdown (LIOB). After the bubble generation via LIOB, a single bubble (radius 5–12 μm) was subsequently trapped stably near the laser focus by the same fs later beam [26,27] (supplemental video S1) which was 500 μm horizontally from the cell (Fig. 1).

### 3.2. Control of a single bubble location relative to the cell membrane

The stably trapped single bubble was then moved horizontally toward the cell by ultrasound pulses (center frequency 7.44 MHz, pulse duration 0.2 μs, pulse repetition frequency 10 KHz, spatial and temporal peak negative pressure 1.4 MPa). Fig. 2A shows an example that illustrates the typical process of spatial control of single bubble. The high speed optical images (Fig. 2A, frames at −16 ms, −8 ms and 0 ms) show that the 7 MHz ultrasound pulses displaced the bubble out of the laser trap and moved it horizontally toward the cell by the acoustic radiation force associated with the ultrasound pulses [33]. The forces acting on the bubble included the acoustic radiation force (horizontal direction toward the cell membrane), the viscous drag force of the fluid opposite, and the buoyancy. The three forces were balanced when the bubble achieved a terminal and constant velocity. The echo signals of the ultrasound pulses (Fig. 2B) from the bubble showed that the bubble (radius 10.5 μm) achieved a terminal velocity of 25 mm/s (V) when the viscous drag force and the buoyancy were balanced by the acoustic radiation force on the bubble. The

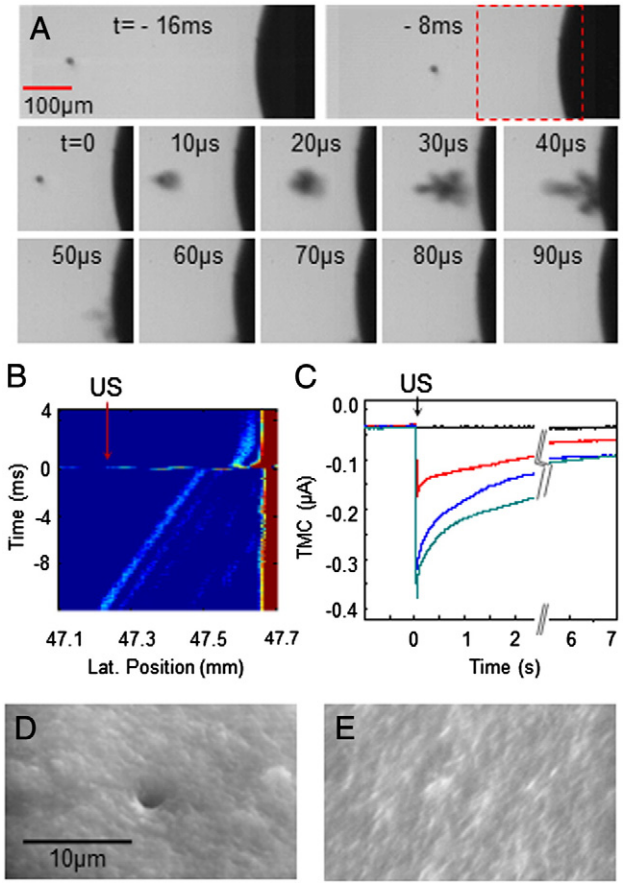


**Fig. 2.** Controlled cavitation of a single bubble increased the cell membrane permeability. (A) Optical images showing the process of a microbubble (radius 10 μm) being pushed toward the cell by the 7.44 MHz pulses. A 1.5 MHz ultrasound (duration of 40 μs) induced collapse of the bubble. (B) The 7.44 MHz M-mode ultrasound image shows the bubble movement and collapse. The 1.5 MHz ultrasound was turned on at t = 0. The horizontal axis represents the distance (mm) from the transducer surface to the bubble. (C) Typical examples of inward TMC during sonoporation generated by 1.5 MHz tone burst with a duration of 13.3 μs (red) or 40 μs (blue) at 1.5 MPa, and duration of 13.3 μs at 1.7 MPa (green). (D) A SEM image showing a pore that was generated on a cell by cavitation of a single bubble in calcium-free ND 96 solution. (E) An example of SEM image of the membrane without pores for the control groups.

buoyancy was calculated to be ~48 pN based on the bubble size, and the viscos drag force was calculated from the Stokes law, $6\pi\mu RV$, where R is the bubble radius, $\mu$ the viscosity, and V the terminal velocity of bubble, to be 4.7 nN. Thus the acoustic radiation force on the bubble was determined from the force balance equation to be 4.9 nN in the horizontal direction in this case. The 7.44 MHz ultrasound pulses did not generate large oscillation and collapse of the bubble because of the higher frequency compared to the resonant frequency of the bubble (0.3–0.5 MHz) with a radius in the range of 5–12 μm, according to the Minneart equation [34].

### 3.3. Cavitation of single bubble and permeation of cell membrane

Once the 7 MHz ultrasound pulses pushed the bubble to reach a desired distance from the cell (indicated by $D/d$ where $D$ is the distance between the bubble and the cell membrane and $d$ the bubble diameter as shown in Fig. 1B), an ultrasound tone burst with center frequency of 1.5 MHz and duration of 13.3 μs or 40 μs was applied at $t=0$ to induce large oscillation and rapid collapse of the bubble (supplemental movie S2) (Fig. 2A, $t>0$ μs), exhibiting the characteristics of an inertial cavitation dominated by the inertia of the sounding fluid. The oscillating/collapsing bubble was also observed to be pushed further toward the cell by the acoustic radiation force generated by the 1.5 MHz ultrasound pulse (Fig. 2A). Corroborated by the bright field images, the collapse of the bubble generated localized impact on the cell and an increase in the inward transmembrane-current (TMC) of the cell (membrane potential clamped at −50 mV) (Fig. 2C), indicating increased membrane permeability as the ions in the extracellular and intracellular spaces flowed across the membrane via electrodiffusion [31,35]. The TMC recovered with a time constant ~3.3 s while the membrane disruption resealed subsequently. No activation of endogenous ion channels was detected.

Scanning electron microscopy (SEM) confirmed the membrane disruption by the collapsing bubble in the form of an isolated pore on the cell membrane (Fig. 2D) from experiments where calcium-free ND 96 solution was used to inhibit the resealing of the pores [31] with other conditions kept the same. In these experiments, the TMC did not recover as expected in calcium-free ND 96 solution. No pores were found in the cells that were not subjected to cavitation or were in ND 96 solution with normal calcium concentration, where the pores should have resealed after 30 s [31,35-38] and the cells were fixed and prepared for SEM examination (*e.g.* Fig. 2E).

### 3.4. Increase in the cell membrane permeability was affected by the distance of the cavitation bubble from the membrane

Experiments were conducted using synchronized monitoring of cavitation and cell membrane permeability to relate the change of TMC with the distance of cavitation bubbles. Fig. 3A–C is the selected example of high-speed images showing the activities of bubble collapse at different distances from the cell membrane. Fig. 3D–F shows the maximum amplitude of changes in TMC vs. the normalized separation distance of bubbles from the cell membrane ($D/d$). The largest increases in the amplitudes of TMC were generated when the 1.5 MHz ultrasound was applied when the bubbles were at the membrane (or $D/d=0$) (Fig. 3). The impact of the cavitation bubble rapidly reduced with increasing$D/d$, with the TMC at $D/d=1$ reduced to half of those at $D/d=0$ and no TMC changes when D/d>3 (Fig. 3D–F).

With the same exposure duration, acoustic pressure of 1.7 MPa produced stronger cavitation than 1.5 MPa (as demonstrated by the larger projection area of the collapsing bubble in Fig. 3B than in 3A) and generated larger changes in TMC (Fig. 3E to compared Fig. 3D). At the same acoustic pressure, ultrasound tone-burst with 40 μs duration produced longer-lasting cavitation activities (Fig. 3C compared to Fig. 3A) and larger TMC values (Fig. 3F) than the 13.3 μs tone burst ultrasound exposures (Fig. 3D).

While TMC decreased with increasing distances in general as the impact of cavitation bubbles reduced, in some cases, large TMC values were generated by the 40 μs exposure (Fig. 3F) when more complex bubble activities were generated. In these cases, it is important to note that the bubbles exhibit more complex dynamic behaviors and that $D/d$, which is the location of the bubble at the start of ultrasound exposure, is no longer an adequate parameter to describe the location of the bubble activities that might occur during a longer exposure time period. As seen in Fig. 3C, during the ultrasound exposure, the bubble first collapsed, grew/expanded further and/or coalesced while being pushed moved toward the cell membrane by the acoustic radiation force, with additional collapse near the membrane (Fig. 3C), which generated a larger amplitude of TMC.

In all of the experiments conducted in this study, most of the cells (>97%) survived after the sonoporation experiment, as indicated by the recovered TMC (short term viability), the normal appearance of the cells, and absence of PI uptake in selected cells after 24–48 h incubation. The TMC for the surviving cells recovered within 20–60 s and maintained the equilibrium level for over 5 min. The cells showed normal appearance without any discoloration after 24–48 h. No PI uptake was detected in all of the cells examined. On the other hand, the cells that lost viability (<3%) were easily identified by non-recovering TMC, membrane discoloration and disintegration, leakage of intracellular contents within 2–5 h [31].

### 3.5. Size of the pores on the membrane vs. the distance of cavitation bubble

Using an electro-diffusion model under a quasi-steady assumption [32], the pore radius corresponding to the maximum amplitude of TMC was calculated for bubbles at various stand-off distances. At $D/d=0$ and 13.3 μs duration, the pore radius was calculated to be $0.106\pm0.032$ μm for 1.5 MPa ($n=70$) (Fig. 4A) and $0.171\pm0.030$ μm ($n=125$) (Fig. 4B) for 1.7 MPa. The radius increased to $0.182\pm0.052$ μm ($n=112$) when the exposure duration was 40 μs (acoustic pressure 1.5 MPa).

### 3.6. Membrane permeation induced by compression of bubble

While inertial cavitation was observed to be the main response to the 1.5 MHz ultrasound exposures at high acoustic pressures and shorter exposure durations (*e.g.* 13.3 μs), translational movement of the bubble induced by acoustic radiation force of the 1.5 MHz can become an important components in ultrasound-driven bubble activities. (Translational movement was the dominant phenomenon for the bubbles influenced by the 7 MHz pulse.) In fact it was observed that the translational movement of bubbles was dominating when much lower acoustic pressure was used (e.g. 0.27 MPa) and when longer duration (*e.g.* >1 ms) was used for the 1.5 MHz ultrasound tone-burst. As shown in Fig. 5, a bubble was first moved toward the cell by the 7 MHz ultrasound pulses and when it reached the cell membrane, 1.5 MHz tone-burst ultrasound at acoustic pressure of 0.27 MPa was applied. Determined by the acoustic field and the bubble size [33], the acoustic radiation force on a bubble of 10.5 μm radius, $F_{radiation}$, was calculated to be 61 nN at an acoustic pressure of 0.27 MPa, much higher than the acoustic radiation force of the 7 MHz (4.9 nN) because of the lower center frequency.

Driven by the 1.5 MHz ultrasound at 0.27 MPa, a bubble oscillated with amplitude in the range of ~1 μm without collapsing (stable cavitation/oscillation) and was pushed by the acoustic radiation force of the 1.5 MHz to compress against the cell membrane (Fig. 5A, Movie S3). This acoustic radiation force can generate a stress of at least 176 Pa on the cell membrane if the cross section area of the bubble was considered as the impact area conservatively.

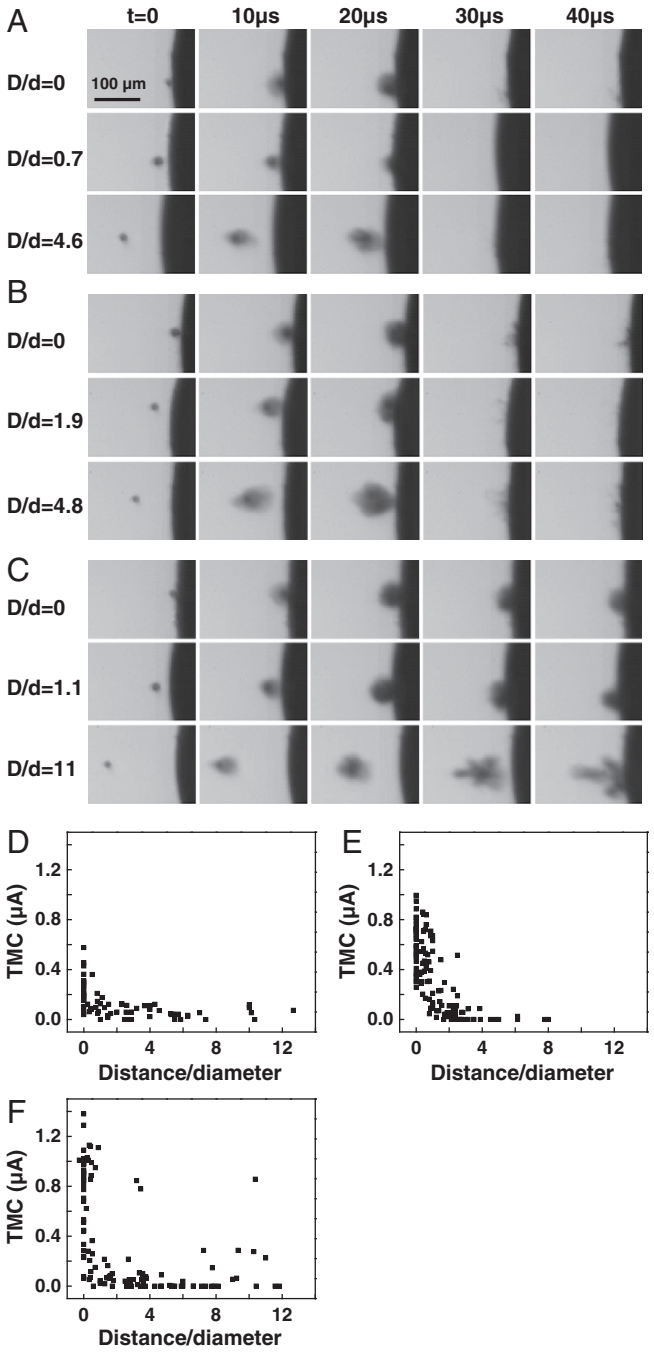


**Fig. 3.** Maximum amplitude of TMC affected by normalized microbubble-membrane distance ($D/d$), acoustic pressure and duration. (A) Typical high speed optical images showing the dynamics of a bubble driven by a 1.5 MHz ultrasound tone burst (duration 13.3 μs, 1.5 MPa). (B) Typical high speed optical images of a bubble driven by a 1.5 MHZ ultrasound tone burst (duration 13.3 μs, 1.7 MPa). (C) Typical high speed optical images of a bubble driven by a 1.5 MHz ultrasound tone burst (40 μs duration, 1.5 MPa). (D)-(F) Scatter plots of the maximum amplitude of TMC corresponding to the ultrasound tone bursts in (A)-(C) vs. $D/d$. The sample sizes were 70, 125 and 112 for (D)–(F) respectively.

Interestingly, the TMC did not change initially as the bubble was beginning to compress the membrane until 70 ms (t = 212 ms) after the start of the 1.5 MHz ultrasound (t = 142 ms). The TMC exhibited an increase (Fig. 5B) at this point (t = 212 ms) when the bubble was seen from the high speed images to be noticeably pushed into the cell membrane. The bubble's sudden engulfment into the cell membrane at this point resembles a local "rupture" of the membrane (position 3 in Fig. 5A, Movie S3). From the force balance relation between the acoustic radiation force and membrane tension (Fig. 5C), $F_{rad} = 2\pi r\gamma_r \sin\theta = \frac{2\pi\gamma_r\left[(d/2)^2 - b^2\right]}{d/2}$, where $b$ is the distance from the bubble center to the membrane at the point of rupture (Fig. 5C), the membrane tension at rupture $\gamma_r$ is estimated to be in the order of 1.23dyn/cm. Ignoring the compressibility of the bubble itself, this localized rupture tension is an order of magnitude lower than the tension for a complete lysis of lipid vesicles [7] or rupture of membrane for mammalian cells [39–41].

The TMC amplitude generated by the rupture corresponded to a pore size of 0.12 μm, which is much smaller than the original radius of the bubble (~10 μm) and a typical glass-rod used in micropipette-based aspiration [42]. At the end of the 1.5 MHz ultrasound exposure, the bubble started to relax back from the membrane with the release of the acoustic radiation force (Fig. 5A), and the TMC started to recover (Fig. 5B, inset), with a time constant similar to that with bubble

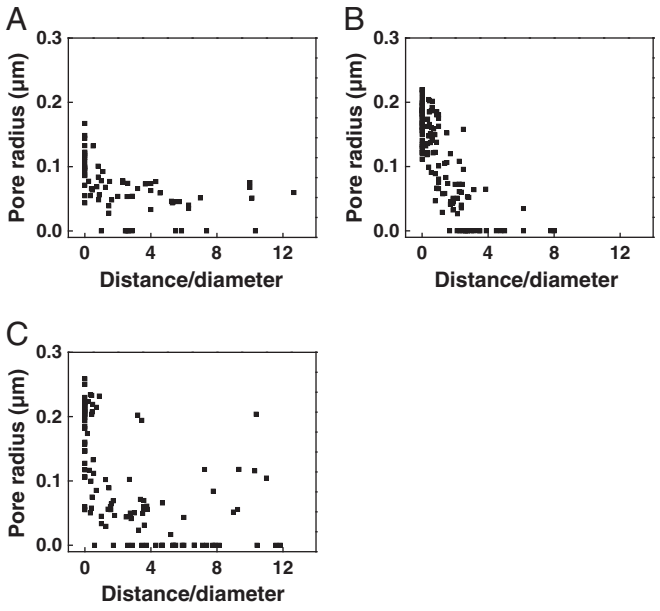


**Fig. 4.** Size of pores generated by cavitation bubble vs. D/d calculated from the values of TMC in Fig. 3. (A) The maximum radius of pores generated by bubbles driven by a 1.5 MPa ultrasound tone burst (1.5 MHz) with duration of 13.3 μs and acoustic pressure of 1.5 MPa. (B) The maximum radius of pores generated by bubbles driven by a 1.5 MHz ultrasound with a duration of 13.3 μs and acoustic pressure of 1.7 MPa. (C) The maximum radius of pores generated by bubbles driven by a 1.5 MHz ultrasound with 40 μs duration and acoustic pressure of 1.5 MPa.

collapse (Fig. 2C). As a note, in this case the shear stress generated by bubble expansion and contraction [8] was calculated to be ~5 Pa, and the shear rate was $2\times10^4/s$.

## 4. Discussion

Although critically important in ultrasound-mediated intracellular delivery by facilitating the disruption of cell membrane and enhancement of barrier permeability [43], no direct evidence has been available to correlate cavitation of microbubble with the increased membrane permeability at the single bubble and single cell level. In this study, we developed a novel approach combining optical, ultrasonic, and electrophysiological techniques to control the spatial location of the microbubble activities relative to the cell and to simultaneously measure the resulting cell response for the first time. This approach provides a unique opportunity to induce controlled impacts on cells and to investigate how cavitation is correlated with the change of cell membrane permeability deterministically. Spatiotemporally correlated results of cavitation bubble and membrane permeability obtained in this study directly demonstrate that the change in membrane permeability was associated with ultrasound driven microbubble activities including collapse or compression of the bubble on the membrane depending on ultrasound amplitude and duration.

### *4.1. Membrane permeation by bubble collapse near the cell membrane*

In our experiments, short ultrasound pulses with relatively high acoustic pressures were used to induce large amplitude (non-linear) oscillation and collapse of the bubble, or inertial cavitation [4,44]. Previous studies have shown the correlation of cavitation and membrane permeation [13,37,45], although no results have been obtained including spatial details of single bubble cavitation. In this study, simultaneous high-speed bright-field imaging and real-time recording of the TMC of a single cell under voltage clamp showed directly that membrane poration was generated by collapse of the bubble and was dependent on spatial location of the microbubbles. Cell membrane permeation (assessed by change of the TMC) and pore formation (assessed by SEM) were only observed when collapse of bubbles occurred near the cell membrane. This indicates that for short duration, ultrasound-induced inertial cavitation generates the membrane permeation.

### *4.2. Effective distance of impact of cavitation on membrane permeation*

The extent of membrane permeation, as assessed by the maximum amplitude of changes in the TMC or the size of pores generated on the membrane, was observed to be significantly affected by the distance of the cavitation bubble (driven by short ultrasound pulse) from the cell membrane. The largest increase in the amplitudes of TMC was generated when the bubble was at the membrane ($D/d=0$) (Fig. 3A). The effect of a collapsing bubble reduced rapidly with increasing distance of the bubble from the cell membrane. The TMC reduced by half when $D/d=0.75$. When the distance of the bubble relative to the diameter of the bubble was larger than 1, the effect of bubble collapse had minimal effect on the TMC. No changes in TMC were observed when $D/d>3$ (Fig. 3D). These observations suggest that a range of effective impact of cavitation may be derived as the stand-off distance when the TMC reduced to half of the maximum values, to be about $D/d=0.75$.

Variation in the TMC values was noted in Fig. 3. The scatter in the data in closer range is mostly due to the variability of individual cells, while the scatter in the larger $D/d$ (Fig. 3F) is due to the complex bubble behaviors driven by the longer exposure time.

These results of the spatial dependence of the cell response to cavitation underscore the importance to realize that ultrasound parameters alone are not sufficient to provide an accurate prediction of sonoporation outcome. Even at the same impact distance, larger acoustic pressures or longer durations generated not only larger impact but also more variation in the change of TMC values, apparently due to the more complex dynamic behaviors of bubbles under these conditions. It is of importance to keep these in mind for sonoporation studies where longer ultrasound pulses are used [46].

### *4.3. Free vs. encapsulated microbubbles driven by an ultrasound field in confined spaces*

Free gas bubbles generated via LIOB were used in this study. The size of the bubble depends on the laser energy and the property of

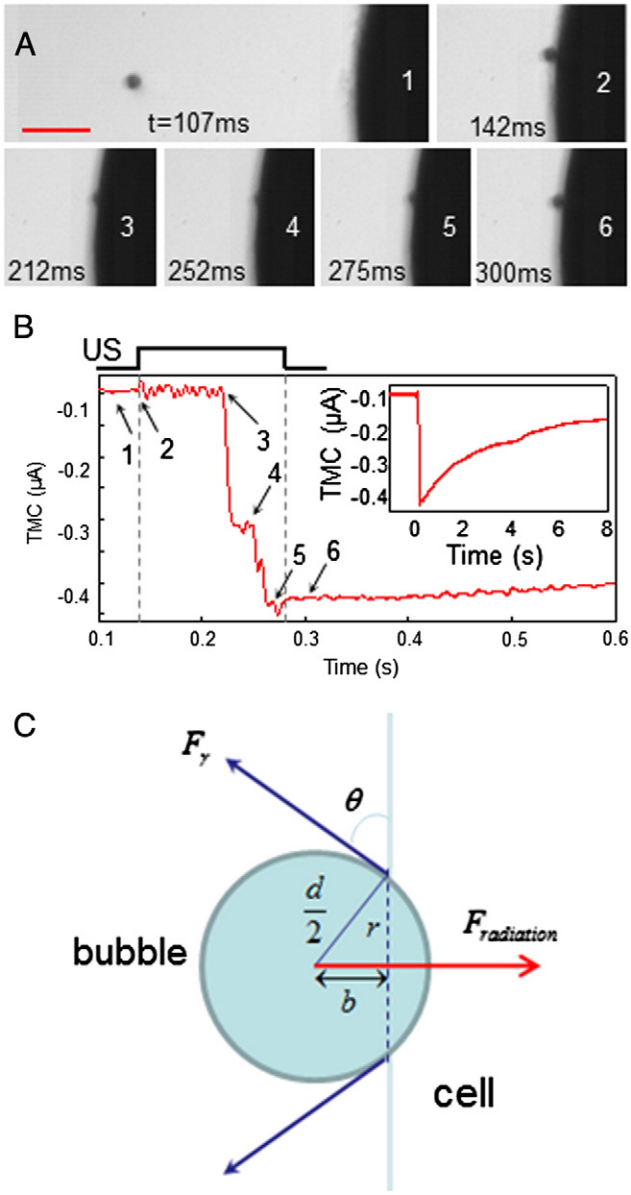


**Fig. 5.** Increase of cell membrane permeability by microbubble compression on the cell membrane. (A) Time-resolved optical images of a bubble moving toward the membrane by the 7 MHz pulses (PRF 10KHz, spatial, temporal peak negative pressure 1.4 MPa) and then pushed against the membrane by a 1.5 MHz ultrasound tone burst (duration 133 ms, peak negative pressure 0.27 MPa). The 1.5 MHz ultrasound pulse was on from frame 2 to 5, and off on frame 6. The scale bar is 100 μm. (B) The TMC of the cell in voltage clamp affected by the ultrasound-driven bubble in (A). The numbers 1 to 6 were time points corresponding to the labeled frames in the optical images in (A). Inset: The recorded TMC showed the recovery of the current in about 8 s. (C) The force balance relation of the acoustic radiation force and the membrane tension on the bubble.

the solution used in the experiment. Variation in the size of the bubbles that were generated depends on the slight fluctuation in the optical properties of the solution. The size range of the bubbles is from 3 to 15 μm, although the stably trapped bubbles are within the rage of 5–12 μm. It is expected that larger bubbles will generate larger impact at the same distance, and bubbles with the same size will generate larger impact when they are closer. Thus the normalized factor $D/d$ is used to provide a uniform parameter.

In many sonoporation studies, encapsulated microbubbles that are pre-made such as the ultrasound imaging contrast agents (e.g. [47]) are often used as cavitation nuclei to facilitate sonoporation (e.g. [9]). For these preformed encapsulated microbubbles, the protecting shell can dampen the response of the microbubbles at least initially because of the shell elastic [48]. Ultrasound exposure may first destroy/fragment the protecting shell [49,50], resulting in free bubbles afterwards which exhibit more robust volume oscillation and/or collapse. Additionally, the cell membrane is the only boundary near the cavitation bubble in this study.

On the other hand, important progress has been made in revealing the details of ultrasound-driven microbubble activities, including particularly, the dynamic behaviors of ultrasound-driven microbubbles within confined spaces such as in vessels [51-54]. The limited dimension of the vessels posts additional spatial boundary and restriction, resulting in different, perhaps more complex, dynamic responses of microbubbles to ultrasound excitation in these cases. These different bubble activities will then in turn generate different effects on the cells within the small vessels.

### 4.4. Membrane permeation by bubble compression on the membrane

When low acoustic pressures (e.g. 0.27 MPa) were used, the 1.5 MHz ultrasound pulse generated stable oscillation of the bubbles with small amplitudes, without causing bubble to collapse. On the other hand, the effect of the acoustic radiation force of the 1.5 MHz ultrasound pulse was dominant when long exposure duration was used. The net force of the radiation force on the bubble pushed the bubble in the direction of the ultrasound propagation (Fig. 1). When the bubble was near the cell, the acoustic radiation force pushed the bubble to compress the cell membrane to cause increasing indentation of the membrane. With continual compression by the bubble, the radiation force and the membrane tension were balanced until disruption of the membrane occurred with the increase of membrane indentation, consistent with the observed delay in the increase of the TMC and corroborated by the high-speed imaging of the bubble movement. The delay in the increase of TMC may be attributed to the viscous-elastic characteristics of the cell membrane.

Cell membrane permeation by bubble compression also allowed the estimation of the membrane tension for localized rupture. From the balance of the acoustic radiation force and the membrane tension, the localized rupture tension was determined to be in the order of 1.23dyn/cm. It is worth noting that the membrane tension depends on the accuracy of measuring b, which was about 0.5–1 μm in this study. The membrane rupture tension is an order of magnitude lower than the tension for a complete lysis of lipid vesicles [7] or rupture of membrane for mammalian cells [39-41]. Although oocytes are much larger than human cells, the size of the cells is not the determining factor in the measurement of the membrane tension at localized rupture in this study. It is possible that the tension at localized membrane rupture or pore formation may be different from the global rupture of membrane or lysis. In addition, the differences of cytoskeletal properties in different cell types might also affect the rupture tension.

It has been previously demonstrated that bubble undergoing small oscillation (stable cavitation) can generate membrane permeation [45]. The study was performed with pulsed ultrasound exposure including short pulses (several μs) with a low duty cycle (~10%). Translational movement induced by the acoustic radiation force was minimal and not observed. In our experiments, a much longer tone-burst ultrasound exposure was used. It is clear from the high-speed imaging observation, the increasing membrane indentation or deformation by the continual ultrasound exposure resulted in increasing membrane tension that eventually caused membrane permeation/disruption. The fact that membrane disruption was observed only after significant membrane deformation by the bubble further supports the notion that bubble compression on the membrane other than the stable oscillation of the bubble caused the membrane permeation in this case. This mechanism of membrane permeation may provide a more realistic description of the sonoporation processes in ultrasound-mediated drug delivery applications when longer exposure but lower acoustic pressures are often

used to avoid inertial collapse of microbubbles in order to reduce undesirable cellular and endothelial damage. It may also be more applicable for sonoporation applications using targeted bubbles that can be attached to the cell membrane by ligand-receptor binding.

### 4.5. Size of the pores on the membrane generated in sonoporation

The size of the pores was in the range of several nm to 200 nm in viable cells. The size range appears to be suitable for intracellular transport of various agents. In sonoporation applications where bubble distance to the cells are not specifically controlled, it is expected a range of pore size will be generated that may have impact on the intracellular delivery efficiency for given agents with different sizes.

The exact values of the pore sizes, which were calculated based on a quasi-static electro-diffusion model relating the pore size with the TMC, presented in here may be specific to this study. However, the results demonstrated in this study illustrate a clear trend and the existence of effective range of cavitation bubbles on the membrane permeation. The cell response to the same impact will depend on the mechanical property of the specific cells used in the study. Thus quantitative study of different cells that may respond differently to same mechanical impact can illustrate the role of membrane property in sonoporation. In addition, the ability to control microbubble activities and measure single cell responses in real-time provides a new venue, besides atomic force microscopy (AFM) or micropipette aspiration [42], to induce controlled impacts on cells and quantify the mechanical properties of live cells dynamically, with possible applications in the studies of cell mechanics, cell characterization and cell manipulation.

Supplementary materials related to this article can be found online at doi:10.1016/j.jconrel.2011.09.068.

## Acknowledgment

This work was supported by the National Institutes of Health (R01CA116592 to C. X. Deng).

## References

[1] D. Luo, W.M. Saltzman, Synthetic DNA delivery systems, Nat. Biotechnol. 18 (2000) 33–37.
[2] N.A. Kootstra, I.M. Verma, Gene therapy with viral vectors, Annu. Rev. Pharmacol. Toxicol. 43 (2003) 413–439.
[3] V.P. Torchilin, Recent approaches to intracellular delivery of drugs and DNA and organelle targeting, Annu. Rev. Biomed. Eng. 8 (2006) 343–375.
[4] W.D. O'Brien Jr., Ultrasound-biophysics mechanisms, Prog. Biophys. Mol. Biol. 93 (2007) 212–255.
[5] J.H. Bang, K.S. Suslick, Applications of ultrasound to the synthesis of nanostructured materials, Adv. Mater. 22 (2010) 1039–1059.
[6] K.S. Suslick, Sonochemistry, Science 247 (1990) 1439–1445.
[7] P. Marmottant, S. Hilgenfeldt, Controlled vesicle deformation and lysis by single oscillating bubbles, Nature 423 (2003) 153–156.
[8] J. Wu, Shear stress in cells generated by ultrasound, Prog. Biophys. Mol. Biol. 93 (2007) 363–373.
[9] P. Prentice, A. Cuschieri, K. Dholakia, M. Prausnitz, P. Campbell, Membrane disruption by optically controlled microbubble cavitation, Nat. Phys. (2005) 107–110.
[10] C.D. Ohl, M. Arora, R. Ikink, N. de Jong, M. Versluis, M. Delius, D. Lohse, Sonoporation from jetting cavitation bubbles, Biophys. J. 91 (2006) 4285–4295.
[11] K. Tachibana, T. Uchida, K. Ogawa, N. Yamashita, K. Tamura, Induction of cell-membrane porosity by ultrasound, Lancet 353 (1999) 1409.
[12] D.L. Miller, S.V. Pislaru, J.E. Greenleaf, Sonoporation: mechanical DNA delivery by ultrasonic cavitation, Somat. Cell Mol. Genet. 27 (2002) 115–134.
[13] Y. Zhou, J. Cui, C.X. Deng, Dynamics of sonoporation correlated with acoustic cavitation activities, Biophys. J. 94 (2008) L51–L53.
[14] T.P. McCreery, R.H. Sweitzer, E.C. Unger, S. Sullivan, DNA delivery to cells in vivo by ultrasound, Methods Mol. Biol. 245 (2004) 293–298.
[15] G. Korpanty, S. Chen, R.V. Shohet, J. Ding, B. Yang, P.A. Frenkel, P.A. Grayburn, Targeting of VEGF-mediated angiogenesis to rat myocardium using ultrasonic destruction of microbubbles, Gene Ther. 12 (2005) 1305–1312.
[16] C.M. Newman, T. Bettinger, Gene therapy progress and prospects: ultrasound for gene transfer, Gene Ther. 14 (2007) 465–475.
[17] P. Hauff, S. Seemann, R. Reszka, M. Schultze-Mosgau, M. Reinhardt, T. Buzasi, T. Plath, S. Rosewicz, M. Schirner, Evaluation of gas-filled microparticles and sonoporation as gene delivery system: feasibility study in rodent tumor models, Radiology 236 (2005) 572–578.
[18] R. Suzuki, K. Maruyama, Effective in vitro and in vivo gene delivery by the combination of liposomal bubbles (bubble liposomes) and ultrasound exposure, Methods Mol. Biol. 605 (2010) 473–486.
[19] S.L. Taylor, A.A. Rahim, N.L. Bush, J.C. Bamber, C.D. Porter, Targeted retroviral gene delivery using ultrasound, J. Gene Med. 9 (2007) 77–87.
[20] Y. Taniyama, K. Tachibana, K. Hiraoka, M. Aoki, S. Yamamoto, K. Matsumoto, T. Nakamura, T. Ogihara, Y. Kaneda, R. Morishita, Development of safe and efficient novel nonviral gene transfer using ultrasound: enhancement of transfection efficiency of naked plasmid DNA in skeletal muscle, Gene Ther. 9 (2002) 372–380.
[21] V.G. Zarnitsyn, M.R. Prausnitz, Physical parameters influencing optimization of ultrasound-mediated DNA transfection, Ultrasound Med. Biol. 30 (2004) 527–538.
[22] H.R. Guzman, D.X. Nguyen, S. Khan, M.R. Prausnitz, Ultrasound-mediated disruption of cell membranes. II. Heterogeneous effects on cells, J. Acoust. Soc. Am. 110 (2001) 597–606.
[23] H.R. Guzman, D.X. Nguyen, S. Khan, M.R. Prausnitz, Ultrasound-mediated disruption of cell membranes. I. Quantification of molecular uptake and cell viability, J. Acoust. Soc. Am. 110 (2001) 588–596.
[24] M. Kinoshita, K. Hynynen, Key factors that affect sonoporation efficiency in in vitro settings: the importance of standing wave in sonoporation, Biochem. Biophys. Res. Commun. 359 (2007) 860–865.
[25] W. Stuhmer, Electrophysiologic recordings from *Xenopus* oocytes, Methods Enzymol. 293 (1998) 280–300.
[26] K. Yang, Y. Zhou, Q. Ren, J.Y. Ye, C.X. Deng, Dynamics of microbubble generation and trapping by self-focused femtosecond laser pulses, Appl. Phys. Lett. 95 (2009) 051107.
[27] J.Y. Ye, G. Chang, T.B. Norris, C. Tse, M.J. Zohdy, K.W. Hollman, M. O'Donnell, J.R. Baker Jr., Trapping cavitation bubbles with a self-focused laser beam, Opt. Lett. 29 (2004) 2136–2138.
[28] P.L. McNeil, R.A. Steinhardt, Plasma membrane disruption: repair, prevention, adaptation, Annu. Rev. Cell Dev. Biol. 19 (2003) 697–731.
[29] P.L. McNeil, T. Kirchhausen, An emergency response team for membrane repair, Nat. Rev. Mol. Cell Biol. 6 (2005) 499–505.
[30] R.A. Steinhardt, The mechanisms of cell membrane repair: a tutorial guide to key experiments, Ann. N. Y. Acad. Sci. 1066 (2005) 152–165.
[31] Y. Zhou, J. Shi, J. Cui, C.X. Deng, Effects of extracellular calcium on cell membrane resealing in sonoporation, J. Control. Release 126 (2008) 34–43.
[32] Y. Zhou, R.E. Kumon, J. Cui, C.X. Deng, The size of sonoporation pores on the cell membrane, Ultrasound Med. Biol. 35 (2009) 1756–1760.
[33] P. Palanchon, P. Tortoli, A. Bouakaz, M. Versluis, N. de Jong, Optical observations of acoustical radiation force effects on individual air bubbles, IEEE Trans. Ultrason. Ferroelectr. Freq. Control 52 (2005) 104–110.
[34] M.S. Plesset, A. Prosperetti, Cavitation and bubble dynamics, Ann. Rev. Fluid Mech. 9 (1977) 145–185.
[35] C.X. Deng, F. Sieling, H. Pan, J. Cui, Ultrasound-induced cell membrane porosity, Ultrasound Med. Biol. 30 (2004) 519–526.
[36] H. Pan, Y. Zhou, O. Izadnegahdar, J. Cui, C.X. Deng, Study of sonoporation dynamics affected by ultrasound duty cycle, Ultrasound Med. Biol. 31 (2005) 849–856.
[37] N. Kudo, K. Okada, K. Yamamoto, Sonoporation by single-shot pulsed ultrasound with microbubbles adjacent to cells, Biophys. J. 96 (2009) 4866–4876.
[38] Y.Z. Zhao, Y.K. Luo, C.T. Lu, J.F. Xu, J. Tang, M. Zhang, Y. Zhang, H.D. Liang, Phospholipids-based microbubbles sonoporation pore size and reseal of cell membrane cultured in vitro, J. Drug Target. 16 (2008) 18–25.
[39] A.S. Goldstein, P.A. DiMilla, Examination of membrane rupture as a mechanism for mammalian cell detachment from fibronectin-coated biomaterials, J. Biomed. Mater. Res. A 67 (2003) 658–666.
[40] R.D. Groot, K.L. Rabone, Mesoscopic simulation of cell membrane damage, morphology change and rupture by nonionic surfactants, Biophys. J. 81 (2001) 725–736.
[41] W. Rawicz, B.A. Smith, T.J. McIntosh, S.A. Simon, E. Evans, Elasticity, strength, and water permeability of bilayers that contain raft microdomain-forming lipids, Biophys. J. 94 (2008) 4725–4736.
[42] R.M. Hochmuth, Micropipette aspiration of living cells, J. Biomech. 33 (2000) 15–22.
[43] C.R. Mayer, N.A. Geis, H.A. Katus, R. Bekeredjian, Ultrasound targeted microbubble destruction for drug and gene delivery, Expert Opin. Drug Deliv. 5 (2008) 1121–1138.
[44] J. Wu, W.L. Nyborg, Ultrasound, cavitation bubbles and their interaction with cells, Adv. Drug Deliv. Rev. 60 (2008) 1103–1116.
[45] A. van Wamel, K. Kooiman, M. Harteveld, M. Emmer, F.J. ten Cate, M. Versluis, N. de Jong, Vibrating microbubbles poking individual cells: drug transfer into cells via sonoporation, J. Control. Release 112 (2006) 149–155.
[46] M. Duvshani-Eshet, L. Baruch, E. Kesselman, E. Shimoni, M. Machluf, Therapeutic ultrasound-mediated DNA to cell and nucleus: bioeffects revealed by confocal and atomic force microscopy, Gene Ther. 13 (2006) 163–172.
[47] R. Bekeredjian, P.A. Grayburn, R.V. Shohet, Use of ultrasound contrast agents for gene or drug delivery in cardiovascular medicine, J. Am. Coll. Cardiol. 45 (2005) 329–335.
[48] V. Sboros, Response of contrast agents to ultrasound, Adv. Drug Deliv. Rev. 60 (2008) 1117–1136.
[49] J.E. Chomas, P. Dayton, J. Allen, K. Morgan, K.W. Ferrara, Mechanisms of contrast agent destruction, IEEE Trans. Ultrason. Ferroelectr. Freq. Control 48 (2001) 232–248.

[50] M. Overvelde, V. Garbin, B. Dollet, N. de Jong, D. Lohse, M. Versluis, Dynamics of coated microbubbles adherent to a wall, Ultrasound Med. Biol. 37 (2011) 1500–1508.
[51] S. Qin, K.W. Ferrara, Acoustic response of compliable microvessels containing ultrasound contrast agents, Phys. Med. Biol. 51 (2006) 5065–5088.
[52] S. Qin, K.W. Ferrara, The natural frequency of nonlinear oscillation of ultrasound contrast agents in microvessels, Ultrasound Med. Biol. 33 (2007) 1140–1148.
[53] P.A. Dayton, K.E. Morgan, A.L. Klibanov, G.H. Brandenburger, K.W. Ferrara, Optical and acoustical observations of the effects of ultrasound on contrast agents, IEEE Trans. Ultrason. Ferroelectr. Freq. Control 46 (1999) 220–232.
[54] H. Chen, W. Kreider, A.A. Brayman, M.R. Bailey, T.J. Matula, Blood vessel deformations on microsecond time scales by ultrasonic cavitation, Phys. Rev. Lett. 106 (2011) 034301.